ORIGINAL RESEARCH

Quantifying Ciliary Dynamics during Assembly Reveals Stepwise Waveform Maturation in Airway Cells

Alina Oltean[1,2], Andrew J. Schaffer[1], Philip V. Bayly[2], and Steven L. Brody[1]

[1]Department of Medicine and [2]Department of Mechanical Engineering and Materials Science, Washington University in St. Louis, St. Louis, Missouri

ORCID ID: 0000-0002-0905-7527 (S.L.B.).

Abstract

Motile cilia are essential for clearance of particulates and pathogens from airways. For effective transport, ciliary motor proteins and axonemal structures interact to generate the rhythmic, propulsive bending, but the mechanisms that produce a dynamic waveform remain incompletely understood. Biomechanical measures of human ciliary motion and their relationships to ciliary assembly are needed to illuminate the biophysics of normal ciliary function and to quantify dysfunction in ciliopathies. To these ends, we analyzed ciliary motion by high-speed video microscopy of ciliated cells sampled from human lung airways compared with primary culture cells that undergo ciliogenesis *in vitro*. Quantitative assessment of waveform parameters showed variations in waveform shape between individual cilia; however, general trends in waveform parameters emerged, associated with progression of cilia length and stage of differentiation. When cilia emerged from cultured cells, beat frequency was initially elevated, then fell and remained stable as cilia lengthened. In contrast, the average bending amplitude and the ability to generate force gradually increased and eventually approached values observed in *ex vivo* samples. Dynein arm motor proteins DNAH5, DNAH9, DNAH11, and DNAH6 were localized within specific regions of the axoneme in the *ex vivo* cells; however, distinct stages of *in vitro* waveform development identified by biomechanical features were associated with the progressive movement of dyneins to the appropriate proximal or distal sections of the cilium. These observations suggest that the stepwise variation in waveform development during ciliogenesis is dependent on cilia length and potentially on outer dynein arm assembly.

Keywords: airway epithelial cell; ciliary beat frequency; dynein; primary ciliary dyskinesia

Motile cilia extend from the apical surface of cells and beat rhythmically to move fluid in the brain, airways, and oviduct (1–3). Similarly, the motile flagella that propel sperm and swimming cells (such as the biflagellate alga *Chlamydomonas reinhardtii*) oscillate with propulsive waveforms to perform their function. In the airway, hundreds of cilia on each cell must beat in coordination to achieve effective mucociliary clearance (4). Ciliary motion is the product of ATP-dependent activation of dynein motor proteins between pairs of microtubule doublets that are the major structural component of the ciliary axoneme (4). Dynein motor complex activity and structural proteins link and stabilize neighboring pairs of microtubule doublets to limit their sliding and produce bending. Mutant *Chlamydomonas* and humans with the genetic motile cilia disease primary ciliary dyskinesia (PCD) demonstrate that failure of production or proper localization of an axonemal motor protein can result in abnormalities in beat frequency or ciliary waveform (5, 6).

(Received in original form December 20, 2017; accepted in final form May 31, 2018)

Supported by National Institutes of Health (NIH) grant HL128370 (S.L.B.) and National Science Foundation grant CMMI-1633971 (P.V.B.). A.O. is a postdoctoral research scholar in the pulmonary science training program (NIH/NHLBI T32HL007317). S.L.B. is the Dorothy and Hubert Moog Professor of Pulmonary Medicine. P.V.B. is the Lilyan and E. Lisle Hughes Professor of Mechanical Engineering. Experiments were performed in part through the Washington University Center for Cellular Imaging, supported by The Children's Discovery Institute of Washington University and St. Louis Children's Hospital (CDI-CORE-2015-505).

Author Contributions: A.O., P.V.B., and S.L.B.: designed experiments; A.O. and A.J.S.: performed experiments; A.O., P.V.B., and S.L.B.: wrote the manuscript.

Correspondence and requests for reprints should be addressed to Steven L. Brody, M.D., Washington University School of Medicine, 660 South Euclid Avenue, Box 8052, St. Louis, MO 63110. E-mail: brodys@wustl.edu.

The uncompressed videos are accessible from this article's supplementary material page.

This article has a data supplement, which is accessible from this issue's table of contents at www.atsjournals.org.

Am J Respir Cell Mol Biol Vol 59, Iss 4, pp 511–522, Oct 2018

Originally Published in Press as DOI: 10.1165/rcmb.2017-0436OC on May 31, 2018
Internet address: www.atsjournals.org

Clinical Relevance

This study examines cilia in *ex vivo* human samples and during ciliogenesis *in vitro*. We quantify cilia waveform in detail and study the relationship of cilia to several other characteristics such as protein localization of dynein arms that are often disrupted in human disease (primary ciliary dyskinesia).

How ciliary proteins direct the waveform remains unresolved. Studies of model organisms have provided insight into the importance of dynein motor proteins for ciliary beat and waveform by manipulating the major motor complexes called the *inner* and *outer dynein arms*, in reference to their position inside the axoneme. In 1973, Gibbons and colleagues showed that chemical removal of the outer dynein arms of flagella in sea urchin sperm halved the beat frequency but qualitatively appeared to have little effect on the waveform shape (7). Similarly, *Chlamydomonas* mutants lacking outer dynein arm components exhibit decreased beat frequency, whereas mutants lacking inner dynein arm components have altered waveform shape (8). Flagellar motion and waveform have been quantified in wild-type and dynein mutants of *Chlamydomonas* to determine parameters such as shear angle, stroke width or amplitude, velocities, and forces exerted on surrounding fluid during swimming (8–10). There are few studies of human ciliary dynamics (11–13). Most of these are detailed studies of a small number of cells and have not explored potential differences between ciliary motion *in vivo* and *in vitro*. Importantly, the normal human ciliary waveform and its development have not been described statistically. Moreover, changes in waveform relative to motor protein incorporation is unknown.

Ciliary waveform analysis is one approach proposed for the diagnosis of PCD (14). Ciliary motion is typically assessed by high-speed video microscopy (HSVM) of cells obtained by fresh biopsy, whereas cells cultured from patient samples have been claimed to be a more accurate tool for diagnosis of ciliopathies (14, 15). The interpretation of HSVM is limited by the fairly subjective description of waveforms, as opposed to rigorous quantitative and statistical analysis, leading to inconsistency between observers and trials (14). For example, on one hand, analysis of ciliary motion often employs qualitative measures such as dyskinesia scores of "abnormal," "stiff," or "asynchronous" beating (16, 17). On the other hand, studies such as those of Papon and colleagues describe human ciliary characteristics in more quantitative terms, such as cilia length, beat angle, the distance traveled by the cilium tip, and duration of the power (or effective) and recovery strokes (12). Sears and coauthors developed tools to fit curves to videos of beating cilia to describe waveform positions, curvature, and velocity and then to form composite waveforms (11). However, isolation and precise quantification of the motion of individual cilia remain challenging, owing to the large number of cilia on each airway cell and the difficulty in resolving structures in videos.

In this study, we used HSVM to obtain quantitative, statistical measures of the human ciliary waveform by *1*) using ciliated cells freshly isolated from human airways and *2*) tracking waveform dynamics in primary culture human airway epithelial cells during ciliogenesis. We uncovered trends in ciliary beat frequency (CBF), length, curvature, and forces between samples in the statistical characterization of the waveform over time. To investigate possible relationships between ciliary dynamics and structural changes during cilia biogenesis, we assessed dynein localization. These studies show that the ciliary waveform develops slowly during ciliogenesis as dynein axonemal proteins are integrated in a multistep process to achieve features of the mature cilia present in human airways.

Methods

Details of the methods are provided in the Supplemental Methods section of the data supplement.

Human Airway Epithelial Cells

The institutional review board at Washington University in St. Louis reviewed the use of human tissues. Human tracheobronchial epithelial cells (hTECs) were isolated from surgical excess of tracheae and proximal bronchi of lungs donated for transplant. For *in vitro* studies, hTECs were expanded on collagen-coated dishes (18, 19), then cultured on collagen-coated membranes (Transwell; Corning) using air–liquid interface (ALI) conditions at first passage.

HSVM

Ciliated airway epithelial cells were placed onto a microscope slide with medium, then covered with a number 1.5 square coverslip (20). Clusters of ciliated cells were imaged on an inverted microscope (Eclipse Ti-U; Nikon) with a high-speed video camera (Ace acA1300-200um; Basler AG) at 37°C with 240 or 360 frames per second. Cultured hTECs were imaged live on Transwell membranes to capture an *en face* view of distal tips of beating cilia. To view the ciliary waveform from the side, cells were imaged on a microscope slide. Mucociliary transport was measured from recordings of microspheres applied to the apical surface of ALI cultures.

CBF and Ciliary Waveform Analysis

CBF was calculated across each video of *ex vivo* or *in vitro* cells using the fast Fourier transform in MATLAB (R2015a; MathWorks). A parameter called *synchrony* was defined using the phase data from the fast Fourier transform analysis.

Cells were selected for cilia length measurements if the full length of cilia was visible and in focus. For waveforms, cilia were manually traced from video recordings of regions typically along the edge of a raft of cells. For each cilium, one beat cycle was traced and fitted using custom MATLAB code to identify the Cartesian coordinates of points and estimate the local angle and curvature (21). Statistics for local angle (θ) and curvature were obtained at each point along the arc length and throughout the beat cycle (21).

Parameters of ciliary dynamics were determined using the equations shown in Table 1. The accumulated bend was calculated as the average of the absolute value of curvature multiplied by length. To describe the amplitude of bending at each time point, the SD of local angles was calculated for each cilium analyzed. This value was averaged to generate the average bend amplitude. Stroke width was defined as the maximum horizontal distance spanned by the waveform. The average force over the entire beat and the maximum force during the power stroke were also estimated (9).

Table 1. Summary of Waveform Parameters and Equations Used to Characterize Each Waveform over One Beat Cycle

Waveform Parameter Name (Reference)	Description	Equation
Stroke width (10, 12)	Maximum distance spanned by the waveform in the *x*-direction	$\max(x) - \min(x)$
Curvature (21)	Derivative of the angle with respect to arc length	$C = \frac{\partial \theta}{\partial s}$
Avg curvature (10)	Average curvature	$\text{avg}(C)$
Accumulated bend (10)	Average, absolute value of curvature multiplied by length (L)	$\text{avg}(\lvert C \rvert)$*L
Avg bending amplitude (present report)	SD of angles at each time, averaged over a cycle	$\text{avg}(\text{SD}(\theta))$
Avg force in *x*-direction (9)	Average of the ciliary force in *x*-direction	$\text{avg}(F_X)$
Max force in *x*-direction (9)	Maximum value of the force in *x*-direction	$\max(F_X)$

Definition of abbreviations: Avg = average; Max = maximum; Min = minimum.

Immunofluorescence Staining and Imaging

Cells on Transwell membranes and from tissue samples (*ex vivo* cells) were immunostained with the following primary antibodies: rabbit anti-DNAH5 (1:400, HPA037470; Sigma-Aldrich), rabbit anti-DNAH9 (1:50, PA5-45744; Thermo Fisher), rabbit anti-DNAH11 (1:50, HPA045880; Sigma-Aldrich), rabbit anti-DNAH6 (1:500, HPA036391; Sigma-Aldrich), and mouse anti-acetylated α-tubulin (1:5,000, clone 6-11B-1; Sigma-Aldrich).

Statistical Analysis

Analysis for statistical significance between groups was assessed with SigmaPlot 11.0 software (Systat Software). Linear regression analyses and *k*-means clustering were performed in MATLAB.

Results

Variation in CBF, Ciliary Synchrony, and Ciliary Length of Cilia from Large Airways

To begin to characterize the human motile ciliary waveform, we first studied motile cilia in *ex vivo* samples obtained directly from excess tracheobronchial tissues of lungs donated for transplant (*see* Table E1 in the data supplement). Cells scraped from the airways were placed on glass slides under coverslips and examined with bright-field HSVM (Figures 1A and 1B, Video E1). The CBF varied between samples, ranging from 3.1 Hz to 19.7 Hz and with an average CBF across all *ex vivo* samples of 9.3 Hz (Figures 1C and 1E); however, only minor differences in SEM were observed among samples from 13 donors (Figure 1F).

To quantify synchronization of cilia within cell clusters, the phase and overall synchrony, representing the relative time at which each cilium begins to move in a new direction, were calculated for each video (Figures 1D and 1G). Selected samples of high and low synchrony were confirmed by kymography (Figure E1, Videos 1 and 2). Synchrony averaged 0.67 across all *ex vivo* samples, signifying that cilia were not beating in perfect unison (i.e., a value of 1.0).

Changes in ciliary length have previously been associated with disease and smoking history (22), suggesting length as an important factor in ciliary function. In our study, the average ciliary length across all *ex vivo* samples was 7.0 μm (Figure 1H). Although ciliary length appeared mostly uniform within a single cell (e.g., Figures E1A and E1D), length varied considerably between cells within each sample and between samples ($P < 0.001$ for ANOVA on ranks). In the tissues analyzed, differences in length were not related to donor smoking history ($P = 0.28$ by *t* test).

Changes in CBF and Ciliary Length during *In Vitro* Ciliogenesis

To investigate changes in ciliary dynamics during ciliary growth, first-passage cultured cells were imaged *en face* for up to 150 days using HSVM for CBF and phase measurements (Figures 2A–2H, Video 3). The onset of beating cilia was observed in most preparations between ALI Days 7 and 14 (Figure 2E). The initial detected CBF exhibited a mean value of 8.3 Hz (range, 3.8–19.4 Hz) at ALI Days 7 through 14, but after ALI Day 14, CBF decreased and approached a fairly constant mean value of 6.0 Hz (range, 2.8–10.8 Hz), which was significantly lower than the average CBF in *ex vivo* samples (9.3 Hz; $P < 0.05$ by one-way ANOVA and Dunn's method). The SE of CBF within each video was highest in the first week of beating and then was consistently decreased across all preparations (Figure 2F). The average CBF measured *en face* at all days, compared with measurements in cells removed from the cultures and imaged from the side on slides (6.8 Hz), was slightly different (Figure E2) ($P = 0.047$ by Mann-Whitney rank-sum test).

Higher CBF in *ex vivo* than in *in vitro* cells suggested that culture conditions might impair CBF. To examine the capability of cultured cells to increase CBF, the apical surface of culture membranes was stimulated by shear stress using a wash with PBS or medium (23). The CBF was transiently increased 3–5 hours later, regardless of the number of days in culture at ALI (Figure 2G). This increase was significantly above baseline but returned to baseline levels the following day. We also considered that treatment with the γ-secretase inhibitor DAPT (*N*-[*N*-(3,5-difluorophenacetyl-L-alanyl)]-*S*-phenylglycine *t*-butyl ester; used to inhibit Notch signaling and increase the number of motile ciliated cells) may affect CBF. Cells were treated for only 2 days between ALI Days 2 and 6, which was before the emergence of cilia. Cilia appeared earlier in preparations that were pretreated with DAPT than in nontreated cultures. Cilia in the DAPT-treated preparations had a higher CBF than nontreated preparations (Figure E3A) (9.0 Hz vs. 5.9 Hz nonzero averages; $P < 0.001$ for Days 7–14 by Mann-Whitney rank-sum test). DAPT added to the medium of a well-differentiated preparation of cells that had attained a stable CBF (ALI Day 33) did not increase CBF during 2 days of treatment or in the 2 weeks after (Figure E3B).

Ciliary length increased in the first month of *in vitro* culture and remained fairly steady but varied within and across samples (Figure 2I). We considered that the CBF was related to ciliary length because

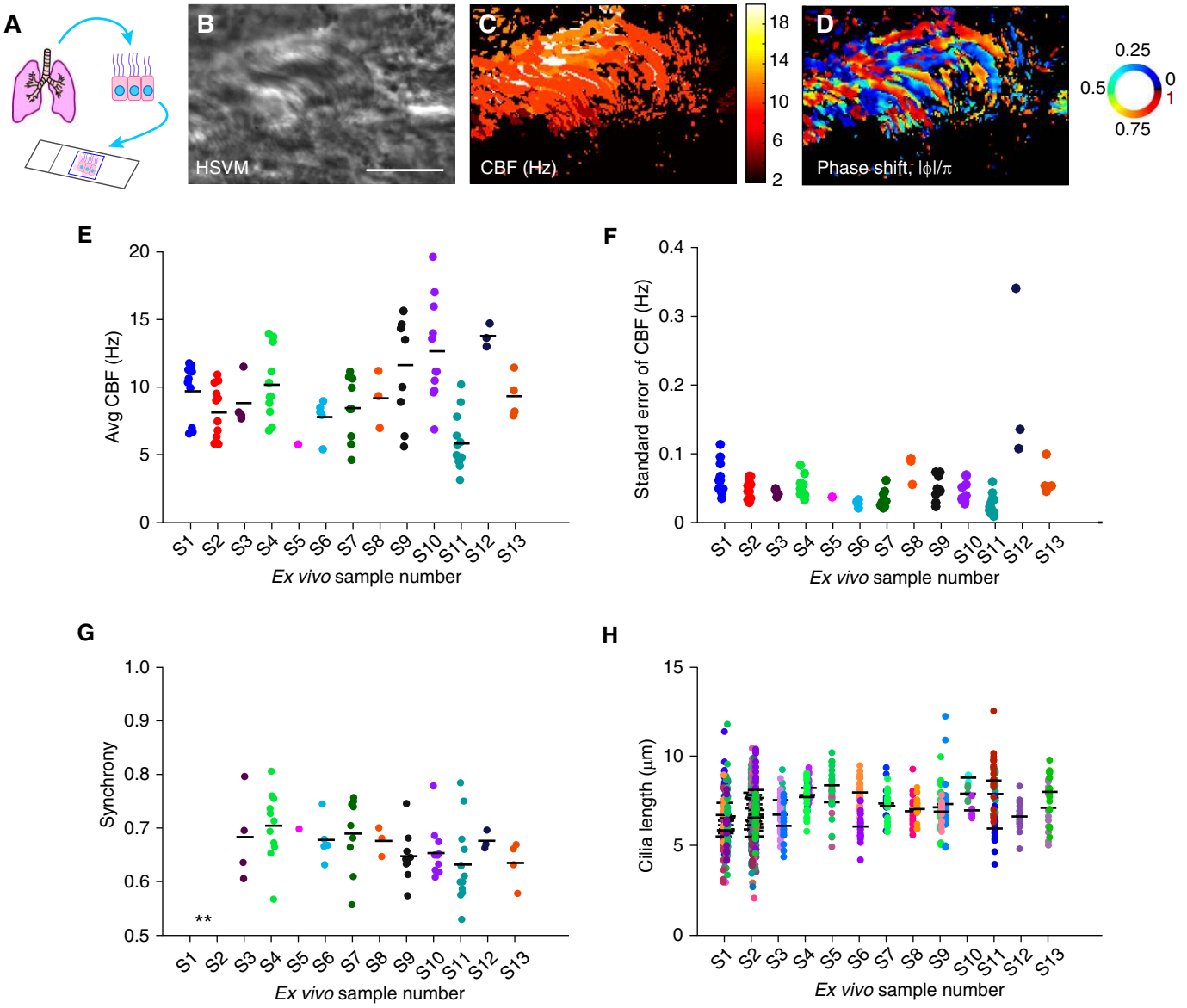

Figure 1. Variability of ciliary beat frequency (CBF) and parameters of *ex vivo* ciliary motion. (*A*) Airway epithelial cells from tracheobronchial segments of human lungs donated for lung transplant were placed under a coverslip for high-speed video microscopy (HSVM). (*B*) Representative video frame of ciliated cells imaged by HSVM (*see* Video 1). (*C*) CBF and (*D*) phase calculated using the fast Fourier transform of the video image in *B*. Color bar in *C* indicates CBF (average value of 10.8 Hz in this video); color wheel in *D* indicates the normalized phase (approximate time delay) of local ciliary motion (synchrony parameter value for this video is 0.74). (*E*) Variation of average CBF in samples (S1–S13; $n = 13$ donors, $n = 95$ total videos). Each point represents the mean of all ciliary motion in each video. Average across all samples is 9.3 Hz. ($P < 0.001$, one-way ANOVA; significant differences exist between seven pairs by Holm-Sidak method). (*F*) SE of CBF within each video for a sample. (*G*) Ciliary beat synchrony calculated as 1 minus the circular SD of the normalized oscillation phase within each video. Mean synchrony of all values is 0.67 ($P = 0.15$ by one-way ANOVA). *Samples excluded owing to short video file length ($n = 73$ total videos). (*H*) Variation in ciliary length in samples. Length was measured in multiple cells for each video. Each color indicates raw data for a single video from a sample ($n = 1{,}349$ measurements, 62 videos). Dunn's *post hoc* test indicates significant differences between 16 pairs ($P < 0.001$, ANOVA on ranks). Black bars indicate mean values in *E*, *G*, and *H*. Scale bar: 10 μm. Avg = average.

mean length of *ex vivo* cilia was greater than in *in vitro* cells (6.9 μm vs. 5.8 μm; $P < 0.001$ by Mann-Whitney rank-sum test). There was no direct correlation between CBF and ciliary length from *ex vivo* or *in vitro* cells analyzed under coverslips (Figure E2). Pretreatment with DAPT did not affect final ciliary length of well-differentiated cells (ALI Day >30; $P = 0.08$ by Mann-Whitney rank-sum test).

The synchrony calculated from the phase of frequency analysis varied considerably across samples (Figure 2H), with a few preparations found to be more synchronized early in ciliogenesis. The mean synchrony across all cultured preparations was only 7.5% higher than observed in *ex vivo* samples (0.72 vs. 0.67; $P < 0.001$ by Mann-Whitney rank-sum test).

Mucociliary transport was assessed by measuring the velocity of microspheres

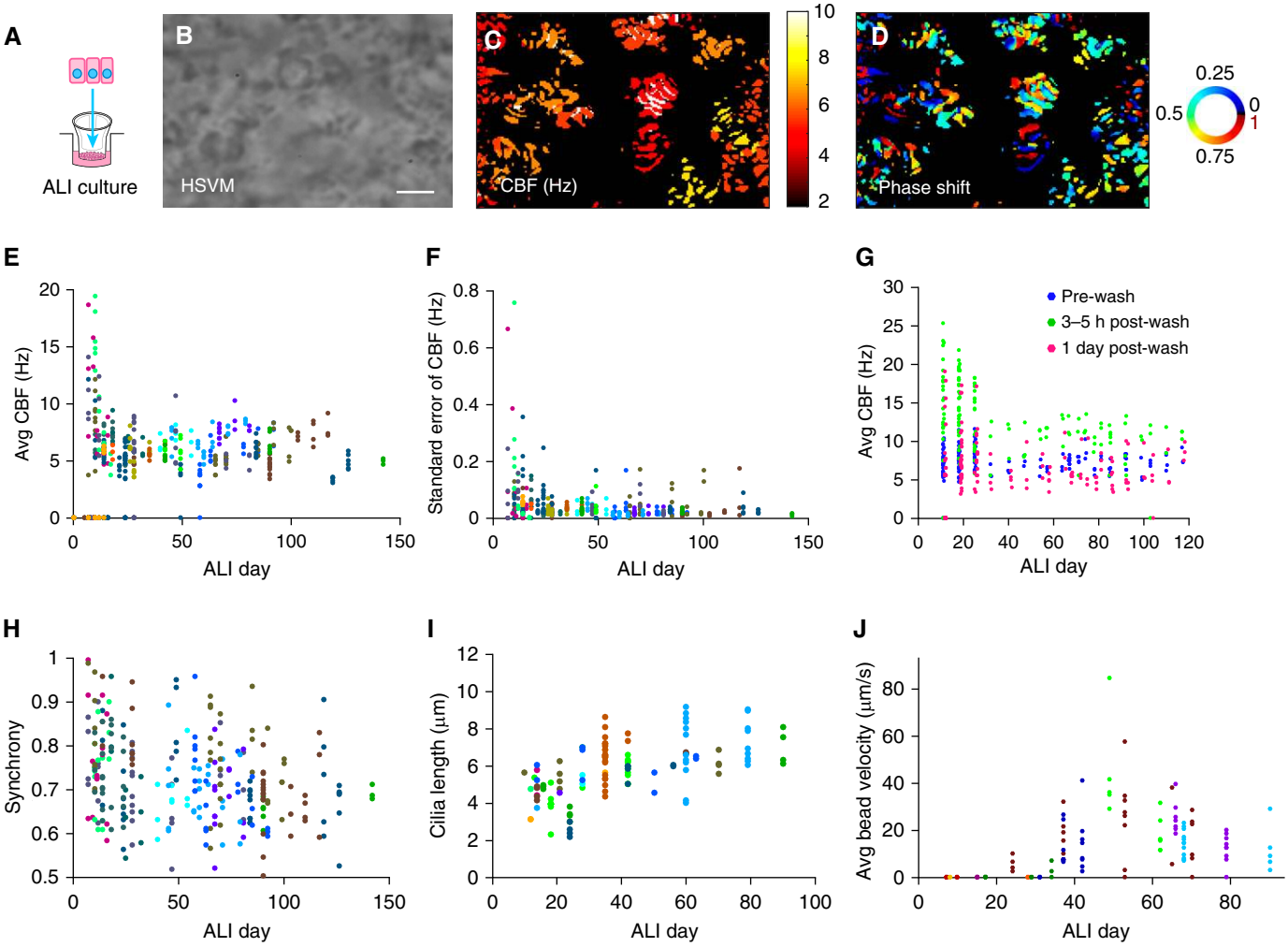

Figure 2. Progression of CBF and length during *in vitro* ciliogenesis. (*A*) Airway epithelial cells isolated from human tracheobronchial segments were expanded on tissue culture plates, then differentiated on supported membranes using air–liquid interface (ALI) conditions. (*B*) Representative frame of cilia on cultured cells imaged *en face* with HSVM at ALI Day 100 (*see* Video 3). (*C*) CBF and (*D*) phase were calculated with the fast Fourier transform of the video in *B*. Color bar in *C* indicates CBF (average of 6.1 Hz in this video); color wheel in *D* indicates the normalized phase (approximate time delay) of the ciliary motion (average synchrony value of 0.68 in this video). (*E*) Variation in average (Avg) CBF for each video during the indicated day of differentiation. Each point represents the average CBF of cells from the entire field. Average of all beating videos is 6.5 Hz ($n = 20$ donors, $n = 505$ total videos with 362 average values >0 Hz). (*F*) SE of each video from *E* ($n = 20$ donors, $n = 362$ total videos). (*G*) The effect of apical medium wash on CBF before and after rinsing. Average CBF values for prewash, 3–5 hours postwash, and the next day are 7.5 Hz, 12.8 Hz, and 6.6 Hz, respectively ($n = 9$ unique donors tested three times with 1 week between each trial; $P < 0.001$ across wash times; $P = 0.008$ across ALI days, two-way ANOVA; Holm-Sidak method indicates significant differences between prewash and 3–5 h postwash, but no significant difference between prewash and 1-day postwash; $n = 428$ total videos). (*H*) Variation in synchrony throughout ciliogenesis ($r^2 = 0.07$; $n = 276$ total videos; $n = 15$ donors). (*I*) Ciliary length in cultured cells sampled from the membrane and imaged under a coverslip as in Figure 1. Average of all values is 5.8 μm ($n = 17$ donors, $n = 125$ videos). (*J*) Mucociliary transport. Mean velocity of microspheres on cell surface for each video ($n = 10$ donors, $n = 126$ total videos). Scale bar: 10 μm. Each color represents the same unique donor in *E*, *F*, *H*, and *I*. A separate cohort of donors was studied in *J*.

applied to the apical surface of ALI preparations. Application of beads increased the CBF (Figure E4), similar to stimulation of the apical surface by washing. Regardless, bead velocity was zero when the cilia first appeared, then gradually increased over the time in culture, with a plateau approximately after ALI Day 40 (Figure 2J).

Comparison of Waveform Analysis of *Ex Vivo* and *In Vitro* Cilia

Cilia generate characteristic waveforms similar to those that have been evaluated comprehensively in wild-type and mutant *Chlamydomonas* using statistical analysis of angle, curvature, and velocity of the flagellum (8, 9, 21). To quantify human ciliary waveform parameters, we analyzed images obtained by HSVM of *ex vivo* and *in vitro* ciliated cells under coverslips. The images from each video were examined across multiple beat cycles to identify, then manually trace, a cilium that was visible for a full beat cycle and visually consistent with other cycles in the video (Figures 3A and E5). Each time point of the traced waveform

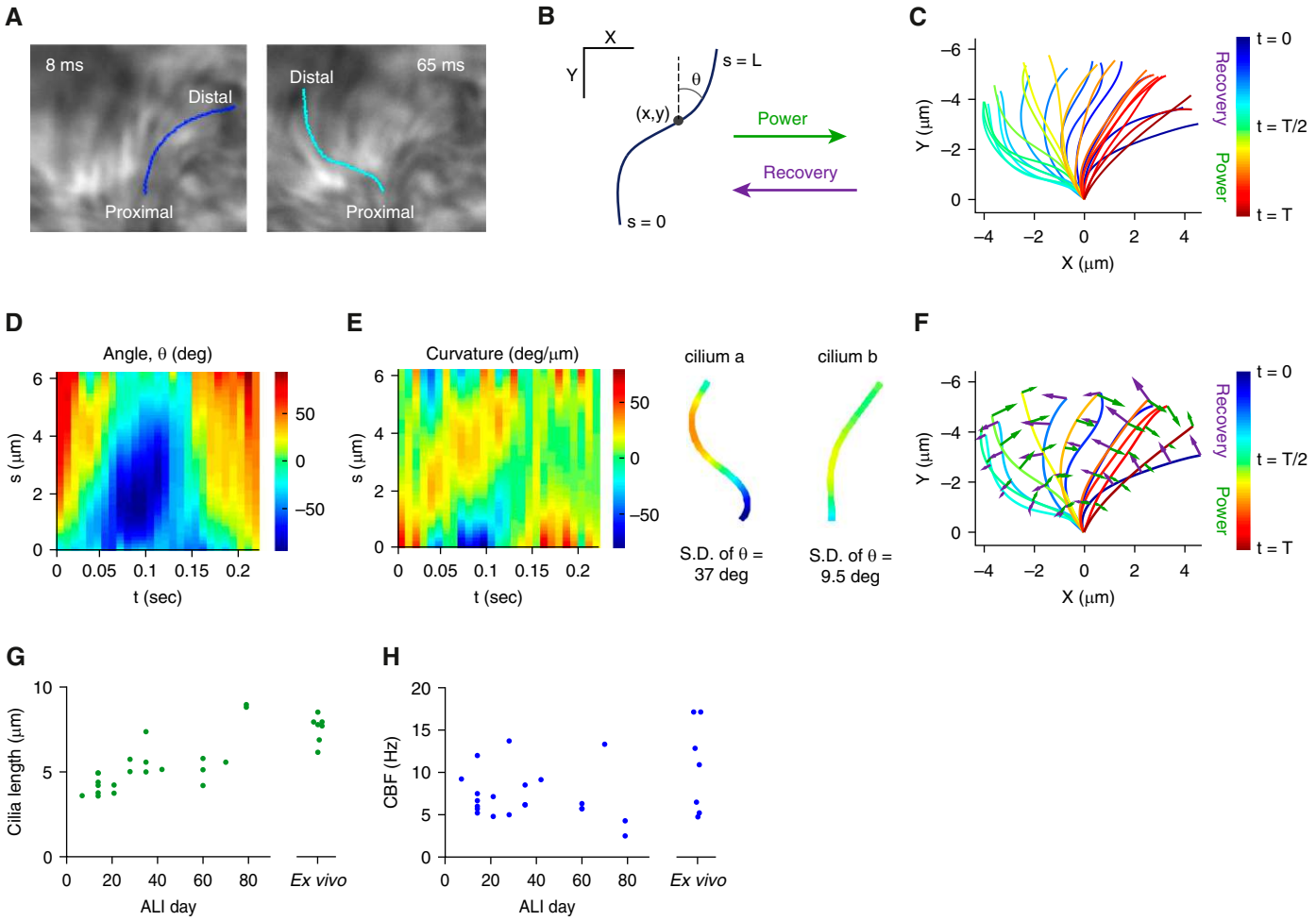

Figure 3. Technique used for analysis of waveforms in *ex vivo* and *in vitro* cilia samples. Ciliary waveforms were analyzed from frames of high-speed video microscopy of *ex vivo* and *in vitro* cells under coverslips. (*A*) Representative example of a manually traced cilium at two time points (8 ms and 65 ms) from frames of a beating cilium in an *ex vivo* sample. (*B*) Traced cilia were fitted with a polynomial function describing angle, θ, in terms of the arc length, s. The tracing was oriented with the power stroke moving in the positive *x*-direction and the recovery stroke in the negative *x*-direction. (*C*) Example of a traced waveform of the *ex vivo* sample shown in *A* for one full beat cycle. Color indicates time in the beat cycle. (*D*) Angle, θ, and (*E*) curvature data, $\partial\theta/\partial s$, for the waveform in *C*. Curvature is shown on two example cilia with the bending amplitude (SD of θ) indicated below. (*F*) Waveform with arrows indicating the local forces exerted by the cilium (arrows in purple = recovery stroke forces and green = power stroke forces; length is proportional to magnitude of force). Only one-half of the time points and one-tenth of the arrows are visualized. (*G* and *H*) Features of all traced waveforms from *in vitro* and *ex vivo* samples indicating the spectrum of (*G*) ciliary length and (*H*) CBF represented in the analyzed waveforms (n = 28 waveforms). deg = degree.

was fit to a curve (Figure 3B) with the power stroke oriented in the positive *x*-direction. The overall waveform (Figure 3C), the angle of each point along the curve (Figure 3D), and the curvature of each point over time (Figure 3E) were determined. The power stroke direction was determined by identifying the time with greatest velocity and positive curvature (*see* example curvature and force vectors in Figures 3E and 3F) (11). The distribution of length and CBF of the cilia analyzed were representative of those observed in *ex vivo* and *in vitro* samples (Figures 3G and 3H).

Changes in Waveform Dynamics during *In Vitro* Ciliogenesis

We hypothesized that the waveform would exhibit changes during ciliary growth and assembly as a function of length and ALI day. To characterize these changes, we investigated waveform parameters previously found to be sensitive to changes in flagellar waveform in *Chlamydomonas*. Such parameters consolidate the spatiotemporal position, angle, curvature, and force data from each waveform into concise, meaningful metrics of ciliary motion (21) (Figures 3 and 4). For example, the stroke width, previously measured in *Chlamydomonas* (10) and human cilia studies (12), describes the distance from start to finish that the tip travels in one beat. The stroke width increased linearly with ciliary length (Figure 4A) in almost a 1:1 proportion (slope of linear best fit is 1.1).

Dysfunctional cilia are frequently described by the qualitative term *stiff* (vs. *normal*) in PCD (24). To capture this qualitative difference in waveform shape, a simple, quantitative metric was sought. First, we averaged the total curvature within each waveform (Figure 4B), which led to values close to 0 owing to the presence

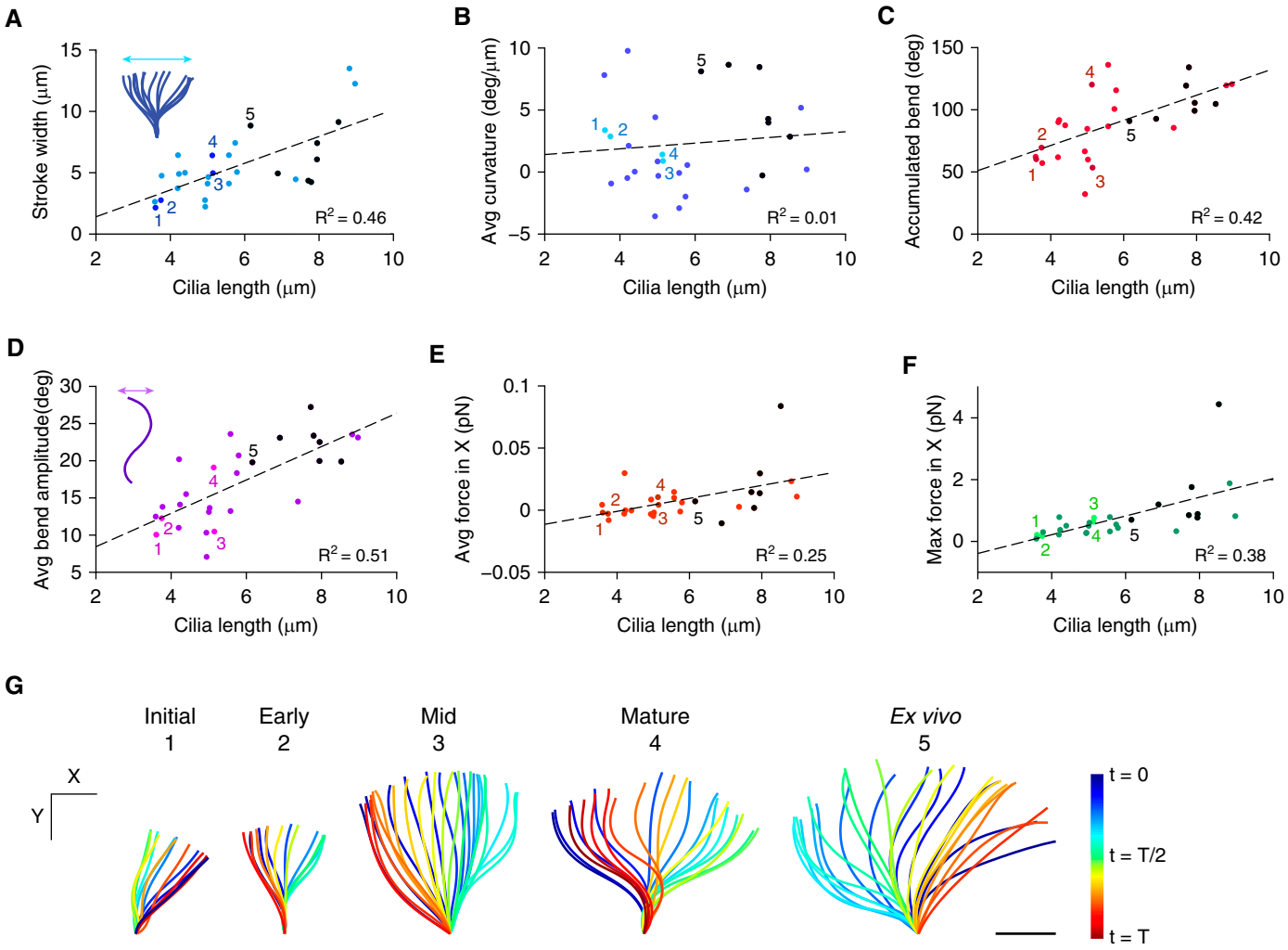

Figure 4. Waveform analysis of cilia during ciliogenesis. Ciliary waveforms from *ex vivo* (filled black circles; $n = 7$) and *in vitro* (filled colored circles; $n = 21$) cell samples were quantified using the indicated waveform parameters; results were analyzed by linear regression (dashed line). (*A*) Stroke width (*see inset*) versus ciliary length (slope = 1.1 μm; $r^2 = 0.46$). (*B*) Average curvature of each waveform versus ciliary length (slope = 0.23 degrees [deg]/μm; $r^2 = 0.01$). Avg = average. (*C*) Accumulated bend for each waveform (slope = 10.1 degrees; $r^2 = 0.42$). (*D*) The average bend amplitude (SD of θ; *see inset*) of waveforms from *in vitro* and *ex vivo* samples as a function of ciliary length (slope = 2.2 degrees; $r^2 = 0.51$). (*E*) The average force (in picoNewtons [pN]) in the *x*-direction relative to ciliary length (slope = 0.0052 pN; $r^2 = 0.25$). (*F*) The maximum force in the power stroke direction relative to ciliary length (slope = 0.30 pN; $r^2 = 0.38$). (*G*) Summary of representative waveforms during four stages of ciliogenesis and an *ex vivo* example. Color bar indicates the relative stroke direction over time (t). Closed circles labeled 1–5 in *A–F* (emphasized by colored shades) indicate data from waveforms in *G*. Scale bar is 2 μm. Mid = midstage.

of positive and negative curvature in the cilia. Subsequently, we calculated the accumulated bend angle, which emphasizes the magnitude of the waveform curvature (10); this metric exhibited a linear relationship with ciliary length (Figure 4C). Finally, we quantified cilium shape by analyzing the variation of angle (θ) data without explicitly incorporating curvature. The SD of θ at each time point produces large values for S-shaped or C-shaped cilia and low values for straight cilia (Figures 3D and 3E). Averaging this SD within each waveform produced the average bend amplitude (Figure 4D), which exhibited a strong linear relationship with ciliary length ($r^2 = 0.51$).

The propulsive force generated by the cilium is one of the key functional parameters of the waveform. Force estimates, obtained using methods previously established in *Chlamydomonas*, showed that average force generated throughout the beat (Figure 4E) and the maximum force in the power stroke (Figure 4F) both increased as a function of ciliary length. The highest values of maximum force typically occurred in *ex vivo* samples, whereas average force was not significantly different between *in vitro* and *ex vivo* samples. We also sought to determine whether beat frequency was related to ciliary waveform. Unlike ciliary length, CBF was not well correlated to waveform metrics ($r^2 < 0.05$ for all waveform parameters, except maximum force with $r^2 = 0.17$). This analysis of ciliary dynamics during growth indicates that *1*) at each time point, a longer cilium exhibits greater total bending; *2*) over a complete cycle, a longer flagellum sweeps across a longer distance; and *3*) the maximum force

of cilia increases as a function of length; but *4*) CBF does not correlate with changes in ciliary dynamics.

Stages of Waveform Development

To compare the maturation of the ciliary waveform to ciliary structure, four stages of waveform development relative to ALI day in culture were identified on the basis of our previous observations (19) and milestones of function noted by others (11, 25). The separation into these stages was supported by similar results via *k*-means clustering of CBF (calculated boundaries at ALI Day 18, ALI Day 35, and ALI Day 67). The *Initial* stage encompasses the period when most cilia begin to beat (ALI Days 7–14). The *Early* stage includes the period of culture when cilia are still growing (ALI Days 15–30). The *Midstage* includes the following 4 weeks of culture at ALI (ALI Days 31–59), and the *Mature* stage includes periods after 2 months of culture (ALI Days 60+). An example of a characteristic waveform from each stage was identified and plotted relative to dynamics of waveforms in each stage (Figure 4G, numbers 1–5 in Figures 4A–4F). These observations suggest that waveforms analyzed at different stages have distinct quantitative features.

Spatial Distribution of Axonemal Dynein during Ciliogenesis

Having identified changes in waveform parameters during ciliary maturation, we sought to determine a relationship to the localization of molecular motors within the ciliary axoneme. Large protein complexes containing dynein motors power the ciliary beat, and genetic mutations affecting individual dynein proteins can alter the waveform in mature cilia, leading to PCD (5). Dynein motor proteins are found in large complexes called the *inner* and *outer dynein arms*, and some distribute within specific regions of the axoneme (26, 27). Their temporal and spatial localization during ciliogenesis is not known. Immunostaining of *ex vivo* cilia for outer arm dyneins showed that DNAH5 was present along the length of the cilia, DNAH9 was typically within the distal portion, and DNAH11 was restricted to the proximal region; inner arm DNAH6 was present along the entire length. These regional patterns are consistent with prior reports (Figure 5A) (26, 28). However, the dyneins did not immediately assume these positions during ciliary growth, but instead slowly localized to these regions over time, corresponding to the identified stages of maturation (Figure 5B, Table E2).

DNAH5 was typically absent, or occasionally variably positioned within the cilia, during the initial stages of *in vitro* ciliogenesis (Figure 5B). In several cells, DNAH5 was visible along basal bodies or within the cytoplasm before entering the

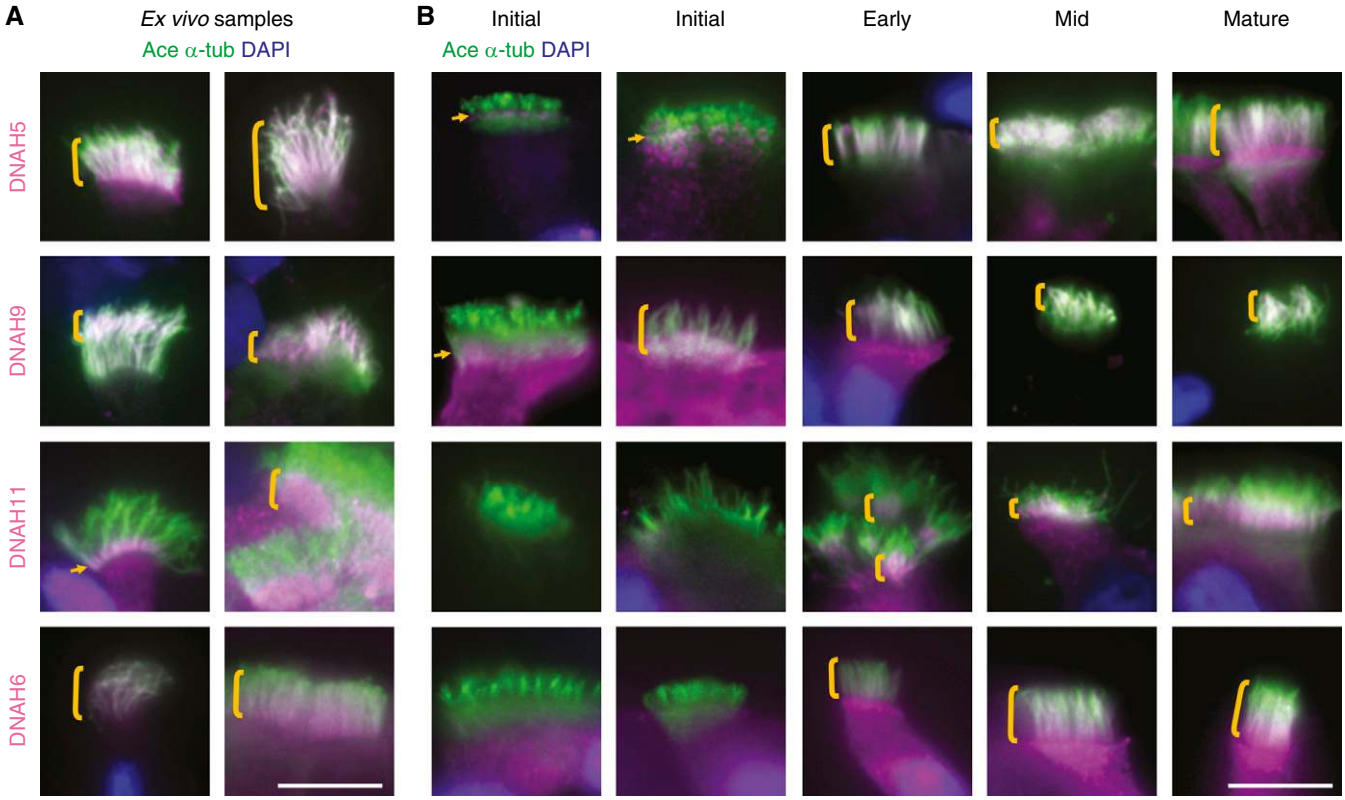

Figure 5. Spatial distribution of axonemal dynein during ciliogenesis. Ciliary location of dynein heavy chain of the outer arm (DNAH5, DNAH9, DNAH11) and inner arm (DNAH6) in (*A*) *ex vivo* and (*B*) *in vitro* cell samples. Representative images from cells immunostained using ciliary marker acetylated α-tubulin (Ace α-tub; green) and the indicated dynein axonemal heavy chain (magenta). Region of colocalization is shown in white. Nuclei were stained with DAPI (blue). Shown are two examples of *ex vivo* cells and, from the *in vitro* preparations, two examples of Initial stage and single examples of Early stage, Mid, and Mature stage. Orange brackets and arrows indicate the position of the dynein within the cilia ($n = 18$ *ex vivo* samples from 8 donors; $n = 67$ *in vitro* samples from 12 donors). Scale bars: 10 μm.

short cilia (Initial stage). By the Early stage, and during the Mature stage, DNAH5 was present throughout the entire cilia. The location of DNAH9 was highly variable, often present throughout the full length of cilia or absent in the cilia of Initial, Early, and Midstage cells, before assuming a distal position in the Mature stage. In contrast, DNAH11 was absent only in the short cilia of the Early stage, but then consistently present with the proximal region at the Early stage, Midstage, and Mature stage. DNAH6 was absent in the cilia at the Initial stage, then present at low levels throughout the cilium length until increasing levels at the Mature stage. DNAH6, DNAH9, and DNAH11 were also present within the cytoplasm, often in the Early stage. These findings may imply that the slow incorporation of dynein proteins contributes to the delayed maturation of an effective waveform *in vitro*.

Relationship of Ciliary Waveform to Assembly

Although dynein arm localization could not be directly compared in the same cells that were live imaged for waveform analysis, we grouped the localization of dynein motors and ciliary motion parameters by stage of ciliary maturation to observe trends and possible correlations (Figures 6A and 6B). DNAH5, DNAH11, and DNAH6 localization of *in vitro* samples resembled *ex vivo* samples in the Early stage of ciliogenesis. However, *in vitro* DNAH9 localization was not distal until the Mature stage. Relationships to waveform parameters revealed that Initial stage cilia had higher CBF than all other stages of *in vitro* culture, but Mature stage cilia did not reach the level of CBF of the *ex vivo* observations in samples, despite proper localization of the dynein heavy chain proteins at this time (Figure 6C). Ciliary length was significantly different between most stages of ciliogenesis (Figure 6D). Mature *in vitro* cilia achieve a length similar to that of *ex vivo* cilia associated with similar localization of all three dynein motor proteins only at this stage.

Four waveform parameters of maturing cilia exhibited a trend toward levels found in *ex vivo* samples. Stroke width generally increased during ciliogenesis but varied substantially during most ciliary stages (Figure 6E); therefore, *ex vivo* stroke width was not significantly different from the stroke width of *in vitro* samples. Average bend amplitude also increased during ciliogenesis (accumulated bend, not shown, exhibited similar trends). Initial stage, Early stage, and Midstage cilia had significantly lower average bend amplitude than *ex vivo* cilia, whereas Mature cilia were nearly identical to *ex vivo* cilia (Figure 6F). Even the earliest cilia had levels of average force that were statistically similar to those of Mature stage and *ex vivo* cilia, suggesting either that cilia are functional even at primitive stages of cilia assembly or that the sample size was too small to detect subtle changes in force. In contrast, the maximum force in the power stroke increased across stages of ciliogenesis with a significant difference between Initial stage cilia and *ex vivo* cilia (Figures 6G and 6H). These findings indicate that there is a distinct pattern of biomechanical maturation of the human ciliary waveform and suggest an association with the assembly of ciliary motor components.

Discussion

The elegant strokes of flagella and cilia have long intrigued scientists, from the first microscopic view of beating cilia in 1675 (29) to the imaging of 9 + 2 axoneme structure in 1949 (30). More recently, knowledge of the components of the ciliary machinery and discovery of diverse genetic causes of motile ciliary disease have motivated the investigation of structure–function relationships, including waveform (31). Assessing ciliary waveform dynamics remains challenging in airway epithelial cells with huge clusters of cilia. Moreover, little is known about how the waveform develops relative to ciliary assembly. As a result, the variation of normal ciliary activity has been addressed primarily and almost solely in terms of beat frequency, and clinical diagnosis still relies heavily on subjective terminology (32). Thus, we addressed two goals: *1*) to characterize biomechanical parameters for the statistical description of the normal waveform and *2*) to determine how these parameters change as cilia assemble. To identify quantitative descriptors of the human ciliary waveform, we analyzed metrics of shape and force during the complete ciliary beat cycle. Statistical measures, in particular the average bend amplitude, captured the maturation of the waveform as cilia grew in culture and became similar to *ex vivo* cilia. The stepwise development of the waveform correlated to key time points in ciliogenesis and the incorporation of dynein arms.

We initially evaluated CBF because it is the most commonly used metric of ciliary function in experimental conditions and for clinical assessment of disease in human samples (15, 24). CBF of *ex vivo* preparations was variable, ranging from 3.1 Hz to 19.7 Hz with statistically significant differences between several donors, suggesting that selecting a representative single value would be difficult. Variations in CBF were noted by others (24, 33, 34). It is possible that CBF varies with the anatomical locations of airway cilia; however, insufficient information is available for this conclusion. Although we made every effort to be consistent in handling samples, CBF may be sensitive to handling and environmental factors such as temperature (35), but it does not appear to be affected by passage number (Figure E6). Overall, large numbers of samples from different individuals and sites must be evaluated to make robust comparisons of CBF.

After examining hundreds of recordings from cultured cells of over 20 different donors, we found that in culture, nascent cilia had a higher beat frequency than at the later stages. After stimulating the surface of *in vitro* preparations with microspheres or medium rinses, the CBF temporarily increased to match CBF of *ex vivo* samples; however, young cilia still maintained the highest CBF. This early elevation of CBF was consistent with measurements of elevated CBF in the tracheas of newborn mice (36), which indicates that the finding is not unique to our culture system. After the early stage high CBF, the average CBF fell and remained stable during ciliogenesis, despite changes in length, waveform shape, and force generation. This finding emphasizes the central role of waveform mechanics, rather than CBF, for assessing ciliary function.

We identified useful quantitative descriptors of the human ciliary waveform by comparing changes in ciliary dynamics during assembly with those observed in *ex vivo* samples. We adapted parameters developed to describe waveforms of flagella of *Chlamydomonas*, sea urchin sperm, and cilia of human airway cells (7, 21, 37).

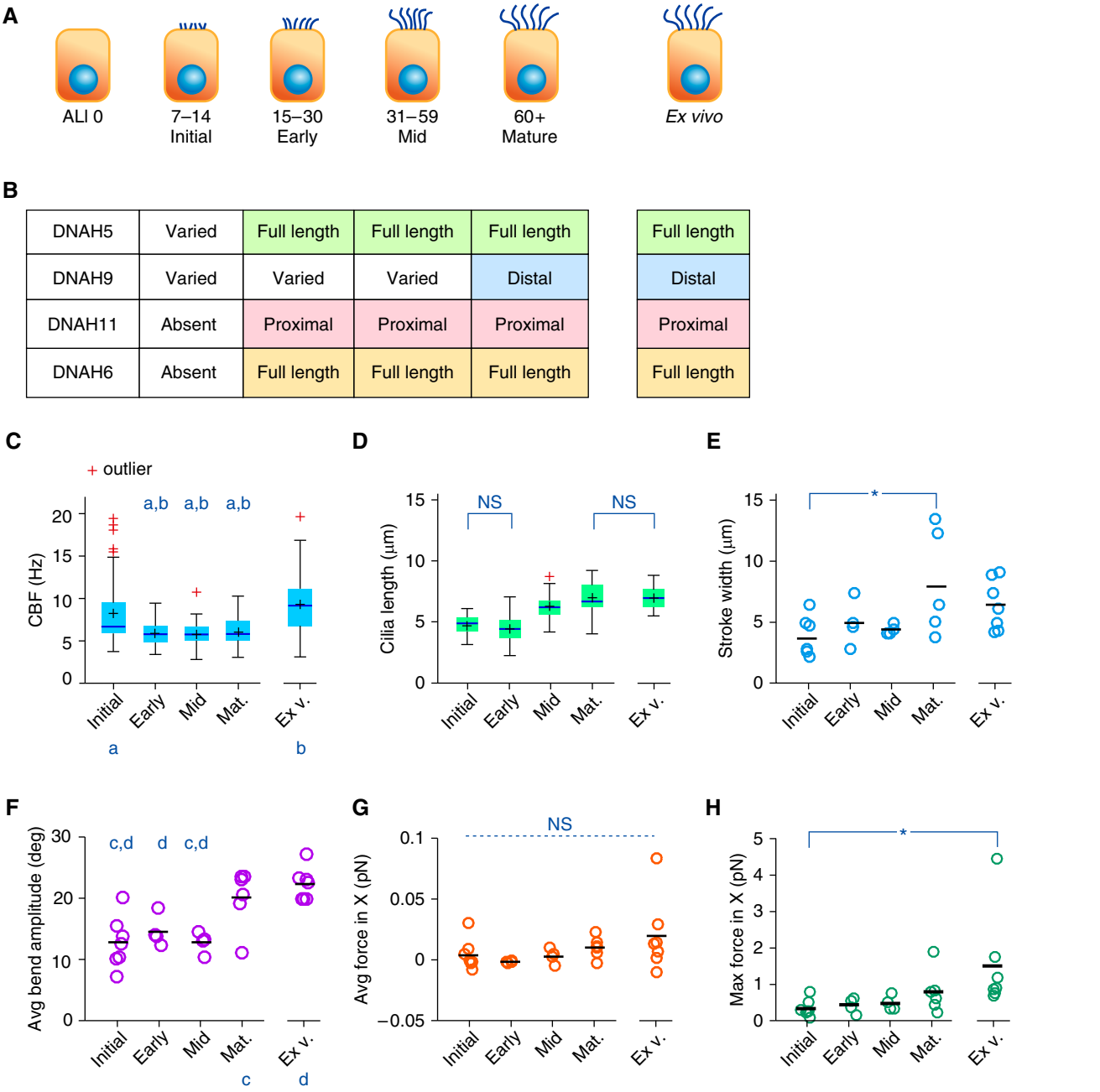

Figure 6. Relationship between ciliary waveform and assembly. (*A*) Drawing of cells during stages of ciliary growth observed *in vitro*, indicated by ALI day, and compared with *ex vivo* cells. (*B*) Trends of dynein localization from fluorescence imaging at each stage of ciliary growth. (*C* and *D*) Changes in CBF and ciliary length corresponding to stages in *A*. Box-and-whisker plot at each stage; box bounds indicate 25th and 75th percentiles. Black marker (+) indicates mean values; red marker (+) indicates outliers (points outside 1.5 times the box height). (*C*) CBF data from Figures 1E and 2E were binned on the basis of ciliary stage ($P < 0.001$, ANOVA on ranks; Dunn's test indicates six pairs with significant differences; "a" indicates a significant difference to Initial stage cilia, and "b" indicates a significant difference from *ex vivo* cilia). (*D*) Ciliary length data from Figures 1H and 2I grouped by ciliary stage ($P < 0.001$, one-way ANOVA; Holm-Sidak method indicates eight pairs of significant differences). NS = not significantly different. (*E–H*) Waveform parameters from Figure 4 grouped by stage. (*E*) Stroke width ($P = 0.042$ for one-way ANOVA; *Holm-Sidak test indicates a significant difference between Initial and Mature stage ciliary stroke width). (*F*) Avg bend amplitude ($P < 0.001$ for one-way ANOVA; Holm-Sidak test indicates five differences; "c" indicates a significant difference from Mature stage cilia, and "d" indicates a significant difference from *ex vivo* cilia). (*G*) Average force (ANOVA on ranks indicates no significant differences; $P = 0.187$). (*H*) Maximum force ($P = 0.006$ for ANOVA on ranks; *Dunn's test indicates a significant difference in maximum horizontal force between Initial stage and *ex vivo* cells). Black bars indicate mean values. Mat. = mature; Ex v. = *ex vivo*.

Among several metrics estimated over the period of waveform maturation, we found the parameter average bend amplitude the most useful and intuitive metric of the shape of the human ciliary waveform. This parameter was not described in prior studies but has specific value as changes in average bend amplitude correlate with increases in ciliary length and the assembly of dynein motor proteins. The average bend amplitude captures both forward and backward bending, in contrast to average curvature, in which positive and negative values cancel arithmetically. This parameter is independent of CBF and appears to reflect changes in maturation, consistent with the stepwise development of bending along the length of the cilium. Clinical use of this measure will depend on improving image acquisition of airway cell waveforms.

An essential component of this work was the acquisition of ciliary waveforms by manual tracing, which is much more difficult in the multiciliated human airway cell than *Chlamydomonas*. Other researchers have reported both the difficulty of manually tracing human cilia waveforms (11) and the variability of ciliary motion in human donors (16). In the latter study of 13 nasal samples from healthy subjects, there was significant variation of qualitative measures of motility and significant interobserver differences (16). We suggest replacing qualitative measures of ciliary waveform shape with quantitative parameters, with the goal of improving the precision of diagnosing PCD with HSVM. Papon and colleagues measured 12 quantitative parameters of ciliary motion (without waveform tracing) in 34 patients being evaluated for PCD (12). Their results included an overall bend angle (correlated to stroke width) and a weighted distance traveled per second at the tip. They reported high sensitivity and specificity of some metrics with respect to clinical diagnosis of PCD. However, the shape of the cilium was not described by values of curvature or bending angles at each time step. These parameters could possibly be quantified and compared at a few key positions during the beat cycle as proposed by Sears and colleagues (11) to quantify shape analysis more efficiently. To speed the overall process, efforts to automate waveform acquisition are ongoing. Quinn and colleagues developed a computational method to automatically assess and classify ciliary motion as healthy or diseased; however, this strategy uses broad classifications of movement (termed by the authors a *black box approach*) with relatively less focus on waveform (38). Upcoming systems should endeavor to combine the benefit of automated algorithms with biophysically relevant descriptors.

Our findings further suggest that comparing human waveforms of airway cilia with the classical waveform models derived from *Chlamydomonas* has limitations as well as implications for understanding ciliary function. For example, our waveform analysis revealed that cilia beat more symmetrically than expected. Some studies have observed small differences in height between the power and recovery strokes (11, 13) that are often exaggerated in diagrams of ciliary beating. More dramatic differences between the power stroke and recovery stroke (as clearly observed in *Chlamydomonas*, where the recovery stroke has a consistent, large bend) would have produced greater average force values during the beat cycle. This suggests that each cilium is less effective than a *Chlamydomonas* flagellum, which uses two flagella to swim. It is consequently reasonable that coordinated motion of multiple cilia is necessary to develop directed flow in the airway. In a sense, this lack of asymmetry "gears down" the force on each cilium and means that each cilium does less work per cycle. Mathematical models of ciliary beating have shown the mechanical efficiency of beating in a metachronal wave (39, 40), which is difficult to measure by mucociliary transport in cultures owing to the "patches" of ciliated cells whose cilia are not oriented in the same direction.

Surveying ciliogenesis *in vitro*, we observed the birth and maturation of the waveform by tracking ciliary growth over time until the ciliary structure and function approached those of *ex vivo* cells. It was unexpected that the maturation of the human waveform biomechanics was relatively slow *in vitro*, requiring 2 months in our culture system to achieve most of the biomechanical and structural features of the cilia studied *ex vivo* from human large airways. Distal, proximal, and full-length dynein proteins in *Chlamydomonas* have also been shown to incorporate at different times in growing flagella, but the effect on waveform has not been determined (41). Dynein arm assembly was associated with waveform maturation, most notably tied to a failure of DNAH9 to achieve a distal position but likely also linked to the assembly of other axonemal proteins. It is possible that the inclusion of distal DNAH9 was particularly important because our findings and those of others show that force is generated in the distal tip, where even a small bend has a large impact.

Our results have two important implications. First, regarding basic ciliary biology, the sequential assembly of the dynein motors over time is contrary to the theory that inner and outer dynein arms are moving in large aggregates into the axoneme (42, 43). Second, as related to PCD, the failure of cilia to generate appropriate curves in the absence of complete dynein incorporation may explain the so-called stiff cilia observed in some PCD mutations (12, 32). One limitation of these findings is that we have not examined the impact of single, specific dynein protein deficiencies on ciliary waveforms; however, this is complex because multiple dynein proteins are often absent in PCD mutations (27, 44).

In conclusion, human motile airway cilia exhibit a wide variety of waveforms and beat frequencies, reflected by substantial variation in quantitative waveform parameters. Analysis during ciliogenesis *in vitro* reveals a stepwise evolution of the maturing waveform. These parameters could be used for the quantitative characterization of cilia in the diagnosis of PCD. In addition, these ciliary waveform parameters can be compared rigorously with predictions from computational models of cilia and flagella to assess underlying hypotheses of dynein activation and illuminate the biophysics of ciliary motility. ■

Author disclosures are available with the text of this article at www.atsjournals.org.

Acknowledgment: The authors thank Amjad Horani, Susan Dutcher, Moe Mahjoub, Mathieu Bottier, and other members of the Washington University cilia group for critical comments.

References

1. Brightman MW, Palay SL. The fine structure of ependyma in the brain of the rat. *J Cell Biol* 1963;19:415–439.
2. Jeffery PK, Reid L. New observations of rat airway epithelium: a quantitative and electron microscopic study. *J Anat* 1975;120:295–320.
3. Dirksen ER. Centriole morphogenesis in developing ciliated epithelium of the mouse oviduct. *J Cell Biol* 1971;51:286–302.
4. Satir P, Sleigh MA. The physiology of cilia and mucociliary interactions. *Annu Rev Physiol* 1990;52:137–155.
5. Knowles MR, Leigh MW, Carson JL, Davis SD, Dell SD, Ferkol TW, *et al*.; Genetic Disorders of Mucociliary Clearance Consortium. Mutations of *DNAH11* in patients with primary ciliary dyskinesia with normal ciliary ultrastructure. *Thorax* 2012;67:433–441.
6. Minoura I, Kamiya R. Strikingly different propulsive forces generated by different dynein-deficient mutants in viscous media. *Cell Motil Cytoskeleton* 1995;31:130–139.
7. Gibbons BH, Gibbons IR. The effect of partial extraction of dynein arms on the movement of reactivated sea-urchin sperm. *J Cell Sci* 1973;13:337–357.
8. Brokaw CJ, Kamiya R. Bending patterns of *Chlamydomonas* flagella: IV. Mutants with defects in inner and outer dynein arms indicate differences in dynein arm function. *Cell Motil Cytoskeleton* 1987;8:68–75.
9. Bayly PV, Lewis BL, Ranz EC, Okamoto RJ, Pless RB, Dutcher SK. Propulsive forces on the flagellum during locomotion of *Chlamydomonas reinhardtii*. *Biophys J* 2011;100:2716–2725.
10. Wilson KS, Gonzalez O, Dutcher SK, Bayly PV. Dynein-deficient flagella respond to increased viscosity with contrasting changes in power and recovery strokes. *Cytoskeleton (Hoboken)* 2015;72:477–490.
11. Sears PR, Thompson K, Knowles MR, Davis CW. Human airway ciliary dynamics. *Am J Physiol Lung Cell Mol Physiol* 2013;304:L170–L183.
12. Papon JF, Bassinet L, Cariou-Patron G, Zerah-Lancner F, Vojtek AM, Blanchon S, *et al*. Quantitative analysis of ciliary beating in primary ciliary dyskinesia: a pilot study. *Orphanet J Rare Dis* 2012;7:78.
13. Bottier M, Blanchon S, Pelle G, Bequignon E, Isabey D, Coste A, *et al*. A new index for characterizing micro-bead motion in a flow induced by ciliary beating: part I, experimental analysis. *PLoS Comput Biol* 2017;13:e1005605.
14. Lucas JS, Barbato A, Collins SA, Goutaki M, Behan L, Caudri D, *et al*. European Respiratory Society guidelines for the diagnosis of primary ciliary dyskinesia. *Eur Respir J* 2017;49:1601090.
15. Jorissen M, Willems T, Van der Schueren B. Ciliary function analysis for the diagnosis of primary ciliary dyskinesia: advantages of ciliogenesis in culture. *Acta Otolaryngol* 2000;120:291–295.
16. Kempeneers C, Seaton C, Chilvers MA. Variation of ciliary beat pattern in three different beating planes in healthy subjects. *Chest* 2017;151:993–1001.
17. Thomas B, Rutman A, O'Callaghan C. Disrupted ciliated epithelium shows slower ciliary beat frequency and increased dyskinesia. *Eur Respir J* 2009;34:401–404.
18. Horani A, Nath A, Wasserman MG, Huang T, Brody SL. Rho-associated protein kinase inhibition enhances airway epithelial basal-cell proliferation and lentivirus transduction. *Am J Respir Cell Mol Biol* 2013;49:341–347.
19. You Y, Richer EJ, Huang T, Brody SL. Growth and differentiation of mouse tracheal epithelial cells: selection of a proliferative population. *Am J Physiol Lung Cell Mol Physiol* 2002;283:L1315–L1321.
20. Bush A, Cole P, Hariri M, Mackay I, Phillips G, O'Callaghan C, *et al*. Primary ciliary dyskinesia: diagnosis and standards of care. *Eur Respir J* 1998;12:982–988.
21. Bayly PV, Lewis BL, Kemp PS, Pless RB, Dutcher SK. Efficient spatiotemporal analysis of the flagellar waveform of *Chlamydomonas reinhardtii*. *Cytoskeleton (Hoboken)* 2010;67:56–69.
22. Leopold PL, O'Mahony MJ, Lian XJ, Tilley AE, Harvey BG, Crystal RG. Smoking is associated with shortened airway cilia. *PLoS One* 2009;4:e8157.
23. Sanderson MJ, Dirksen ER. Mechanosensitivity of cultured ciliated cells from the mammalian respiratory tract: implications for the regulation of mucociliary transport. *Proc Natl Acad Sci USA* 1986;83:7302–7306.
24. Chilvers MA, Rutman A, O'Callaghan C. Ciliary beat pattern is associated with specific ultrastructural defects in primary ciliary dyskinesia. *J Allergy Clin Immunol* 2003;112:518–524.
25. Hill DB, Button B. Establishment of respiratory air-liquid interface cultures and their use in studying mucin production, secretion, and function. *Methods Mol Biol* 2012;842:245–258.
26. Dougherty GW, Loges NT, Klinkenbusch JA, Olbrich H, Pennekamp P, Menchen T, *et al*. DNAH11 localization in the proximal region of respiratory cilia defines distinct outer dynein arm complexes. *Am J Respir Cell Mol Biol* 2016;55:213–224.
27. Fliegauf M, Olbrich H, Horvath J, Wildhaber JH, Zariwala MA, Kennedy M, *et al*. Mislocalization of DNAH5 and DNAH9 in respiratory cells from patients with primary ciliary dyskinesia. *Am J Respir Crit Care Med* 2005;171:1343–1349.
28. Li Y, Yagi H, Onuoha EO, Damerla RR, Francis R, Furutani Y, *et al*. *DNAH6* and its interactions with PCD genes in heterotaxy and primary ciliary dyskinesia. *PLoS Genet* 2016;12:e1005821.
29. Gibbons IR. Cilia and flagella of eukaryotes. *J Cell Biol* 1981;91:107s–124s.
30. Grigg GW, Hodge AJ. Electron microscopic studies of spermatozoa I. The morphology of the spermatozoon of the common domestic fowl (*Gallus domesticus*). *Aust J Biol Sci* 1949;2:271–286.
31. Satir P, Christensen ST. Overview of structure and function of mammalian cilia. *Annu Rev Physiol* 2007;69:377–400.
32. Raidt J, Wallmeier J, Hjeij R, Onnebrink JG, Pennekamp P, Loges NT, *et al*. Ciliary beat pattern and frequency in genetic variants of primary ciliary dyskinesia. *Eur Respir J* 2014;44:1579–1588.
33. Hirst RA, Jackson CL, Coles JL, Williams G, Rutman A, Goggin PM, *et al*. Culture of primary ciliary dyskinesia epithelial cells at air-liquid interface can alter ciliary phenotype but remains a robust and informative diagnostic aid. *PLoS One* 2014;9:e89675.
34. Veale D, Rodgers AD, Griffiths CJ, Ashcroft T, Gibson GJ. Variability in ciliary beat frequency in normal subjects and in patients with bronchiectasis. *Thorax* 1993;48:1018–1020.
35. Clary-Meinesz CF, Cosson J, Huitorel P, Blaive B. Temperature effect on the ciliary beat frequency of human nasal and tracheal ciliated cells. *Biol Cell* 1992;76:335–338.
36. Francis RJB, Chatterjee B, Loges NT, Zentgraf H, Omran H, Lo CW. Initiation and maturation of cilia-generated flow in newborn and postnatal mouse airway. *Am J Physiol Lung Cell Mol Physiol* 2009;296:L1067–L1075.
37. Friedrich BM, Riedel-Kruse IH, Howard J, Jülicher F. High-precision tracking of sperm swimming fine structure provides strong test of resistive force theory. *J Exp Biol* 2010;213:1226–1234.
38. Quinn SP, Zahid MJ, Durkin JR, Francis RJ, Lo CW, Chennubhotla SC. Automated identification of abnormal respiratory ciliary motion in nasal biopsies. *Sci Transl Med* 2015;7:299ra124.
39. Bottier M, Peña Fernández M, Pelle G, Isabey D, Louis B, Grotberg JB, *et al*. A new index for characterizing micro-bead motion in a flow induced by ciliary beating: part II, modeling. *PLoS Comput Biol* 2017;13:e1005552.
40. Elgeti J, Gompper G. Emergence of metachronal waves in cilia arrays. *Proc Natl Acad Sci USA* 2013;110:4470–4475.
41. Yagi T, Uematsu K, Liu Z, Kamiya R. Identification of dyneins that localize exclusively to the proximal portion of *Chlamydomonas* flagella. *J Cell Sci* 2009;122:1306–1314.
42. Fowkes ME, Mitchell DR. The role of preassembled cytoplasmic complexes in assembly of flagellar dynein subunits. *Mol Biol Cell* 1998;9:2337–2347.
43. Kobayashi D, Takeda H. Ciliary motility: the components and cytoplasmic preassembly mechanisms of the axonemal dyneins. *Differentiation* 2012;83:S23–S29.
44. Horani A, Ferkol TW, Dutcher SK, Brody SL. Genetics and biology of primary ciliary dyskinesia. *Paediatr Respir Rev* 2016;18:18–24.